Hardening and strengthening behavior in rate-independent strain gradient crystal plasticity

Nellemann, C.; Niordson, C. F. ; Nielsen, K.L.

Published in:
European Journal of Mechanics A - Solids

Link to article, DOI:
10.1016/j.euromechsol.2017.09.006

Publication date:
2018

Document Version
Peer reviewed version

Hardening and Strengthening Behavior in Rate-Independent Strain Gradient Crystal Plasticity

C. Nellemann[a,1,*], C.F. Niordson[a], K.L. Nielsen[a]

[a]*Department of Mechanical Engineering, Solid Mechanics, Technical University of Denmark, DK-2800 Kgs. Lyngby, Denmark*

Abstract

Two rate-independent strain gradient crystal plasticity models, one new and one previously published, are compared and a numerical framework that encompasses both is developed. The model previously published is briefly outlined, while an in-depth description is given for the new, yet somewhat related, model. The difference between the two models is found in the definitions of the plastic work expended in the material and their relation to spatial gradients of plastic strains. The model predictions are highly relevant to the ongoing discussion in the literature, concerning 1) what governs the increase in the apparent yield stress due to strain gradients (also referred to as strengthening)? And 2), what is the implication of such strengthening in relation to crystalline material behavior at the micron scale? The present work characterizes material behavior, and the corresponding plastic slip evolution, by use of the finite element method. The pure shear problem of an infinite material slab is investigated, with the previously published model displaying strengthening, while the new model does not. In addition to the numerical approach an exact closed form solution, to the pure shear problem, is obtained for the new model, and it is demonstrated that the model predicts proportional straining in the entire plastic regime. Somewhat surprising it is found that the predictions for strain gradient hardening

*Corresponding author
Email address: chnel@mek.dtu.dk (C. Nellemann)
URL: http://orcid.org/0000-0002-9677-1285 (C. Nellemann)
[1]Tel: +45 4525-4263, Fax: +45 4593-1475

coincide for the two models.

Keywords: Strain gradient crystal plasticity, Strengthening, Hardening

1. Introduction

Formulating strain gradient plasticity theories, without compromising thermodynamics or allowing temporal discontinuities in key stress measures, has been and continues to be, a great challenge to the scientific community. The general experimental trend that *smaller is stronger* is well-established (Greer and Hosson, 2011), but conclusive experiments are yet to unveil if the effect of strain gradients gives rise to additional hardening, strengthening, or a combination of the two. This work defines strengthening as an apparent delay in plastic flow, while hardening is defined by the combined effect of conventional strain hardening and the additional hardening related to gradients of plastic strain. Recent experiments display evidence of a strengthening behavior in polycrystalline wires under cyclic loading (Liu et al., 2015), and in the average compressive load for thin confined copper films (Mu et al., 2014). However, in the majority of micron-scale experiments (e.g. nano-indentation and torsion Ma and Clarke, 1995; Guo et al., 2017, respectively), the complexity of the deformation obscures whether the size dependent observations link to hardening, strengthening, or both. With off-set in isotropic theories, Fleck et al. (2015) recently brought new insight into how the mathematical structure of theories influences the predicted material behavior, in their work entitled "Guidelines for Constructing Strain Gradient Plasticity Theories". Fleck et al. (2015) focus on the apparent elastic gap at initial yield (referred to as strengthening in the present work) that results from a number of existing theories. Their intention is not to remedy theories, but rather to understand the underlying mathematical structure governing this effect. Distinct changes to the predicted material behavior are found for slight modifications to the definition of plastic work expended in the material. By leaving out the enrichment of strain gradients in the lowest order contribution to the plastic work, the model prediction is shown

to preclude strengthening behavior. The present work intends to extend these guidelines to crystal plasticity. Following the findings of Fleck et al. (2015), the present work takes as off-set the three key objectives, for "proper model development", put forward by Hutchinson (2012). That is, the proposed theoretical framework has to;

1) reduce to that of conventional J_2 plasticity theory in the limit of sufficiently small strain gradients.

2) take as input the elastic material properties, the uni-axial tensile relation between stress and plastic strain, and a length parameter to characterize the gradient effects.

3) coincide with J_2 deformation theory, with same inputs, throughout a proportional straining history.

In Nellemann et al. (2017), the development of an "easy-to-treat" rate-independent model of strain gradient plasticity, which followed the theory of Hutchinson (2012), proved somewhat complicated to handle in a numerical framework (referred to as Model A in the present work). In contrast to this the new model proposed in the present work (referred to as Model B) is shown to obey all three objectives, demonstrating the following features; 1. no strengthening is predicted, such that initial yield occurs at the conventional yield stress, whereby strain gradients only contribute to hardening. As a consequence, 2. the proposed model predicts proportional straining in the entire plastic regime and, hence, allows for an exact closed form solution to be developed for the pure shear problem investigated. Moreover, both models take as input; elastic parameters, a relation between the resolved shear stress and the slip and a material length parameter, following objective 2). It is emphasized that the three objectives above are highlighted since they are desirable features of rate-independent plasticity theories, which allow for an analytical treatment of a proposed framework. Objective 3) only speaks to model predictions which display proportional straining. The theories developed will involve directional derivatives of higher

order stresses that may be interpreted as back-stresses which influence model predictions under general loading conditions. The constitutive nature of these higher order stresses determine whether gradient effects arise as strengthening, hardening or a combination of the two. In the present work, Model B is compared to Model A, and the differences between the two models are emphasized. The present research extends the findings of Fleck et al. (2015) regarding strengthening behavior of an isotropic solid to crystal plasticity. The paper is structured as follows. The proposed strain gradient crystal plasticity framework is outlined in Section 2, where two different approaches to defining the plastic work expended in the material are presented. Section 3 lays out the numerical model, and Section 4 presents the pure shear problem considered along with a closed form solution. Numerical results are given in Section 5 and a direct comparison to the exact solution is demonstrated. Finally, concluding remarks are given in Section 6.

2. Strain gradient crystal plasticity

One unified framework for rate-independent strain gradient crystal plasticity that encompasses both the model (Model A) from Nellemann et al. (2017) and a new and improved model (Model B), is presented in Section 2.1. The definition of the plastic work expended in the material constitutes the only difference between the two models and both mathematical formulations will be discussed. Following the definitions of the plastic work expressions, their incremental counterparts are presented in Section 2.2. The presentation is limited to the assumption of monotonic loading, which allows for a brief presentation of the models, that preserves the characteristics relevant to the current investigation. The reader is referred to Nellemann et al. (2017) for further details on the derivation presented throughout Section 2.

Throughout, tensor notation is adopted and repeated lower case Latin indices imply summation, whereas comma separation implies spatial derivatives. Quantities denoted by superscript Greek letters refers to a specific slip system, while

all active slip systems are indicated by the superscript (:). The $\dot{(\ )}$ notation indicates an incremental quantity and a function is indicated by hard brackets e.g. $f[*]$.

2.1. Modeling framework

The present work is restricted to small stain rate-independent material behavior, where u_i are the displacements, $u_{i,j}$ are the spatial gradient of the displacements, and $\varepsilon_{ij} = (u_{i,j} + u_{j,i})/2$ are the total strains. The Cauchy stress is given by the elastic relation; $\sigma_{ij} = L^e_{ijkl}\varepsilon^e_{kl}$, where L^e_{ijkl} is the isotropic elastic stiffness tensor and ε^e_{ij} denotes the elastic strain determined by the total strain and the plastic strain, ε^p_{ij}, as; $\varepsilon^e_{ij} = \varepsilon_{ij} - \varepsilon^p_{ij}$. In accordance with the strain gradient crystal plasticity framework initially proposed by Gurtin (2000), the equations of equilibrium read

$$\sigma_{ij,j} = 0 \tag{1}$$

$$q^{(\alpha)} - \tau^{(\alpha)} - \xi^{(\alpha)}_{,i} s^{(\alpha)}_i = 0 \tag{2}$$

with the conventional equilibrium given by Eq. (1) and the microforce equilibrium given by Eq. (2). Here, the Cauchy stress, σ_{ij}, is work conjugate to the elastic strain, the micro-stress, $q^{(\alpha)}$ (the sum of a recoverable part, $q^{R(\alpha)}$, and a dissipative part, $q^{D(\alpha)}$), is work conjugate to the slip, $\gamma^{(\alpha)}$, and the higher order stress, $\xi^{(\alpha)}$, is work conjugate to the normalized pure edge dislocation density (neglecting screw dislocations) $\gamma^{(\alpha)}_{,i} s^{(\alpha)}_i$. The normalized dislocation density is also known as the net Burgers vector density. The resolved shear stress on a slip system is; $\tau^{(\alpha)} = \sigma_{ij}\mu^{(\alpha)}_{ij}$, with the Schmid orientation tensor $\mu^{(\alpha)}_{ij}$ given by Eq. (3).

In the adopted crystal plasticity framework, the plastic strain relates to the crystallographic slip, $\gamma^{(\alpha)}$, on individual slip systems through the relation

$$\varepsilon^p_{ij} = \sum_{(\alpha)} \gamma^{(\alpha)} \mu^{(\alpha)}_{ij}, \quad \text{with} \quad \mu^{(\alpha)}_{ij} = \frac{1}{2}\left(s^{(\alpha)}_i m^{(\alpha)}_j + s^{(\alpha)}_j m^{(\alpha)}_i\right) \tag{3}$$

with a specific slip system, α, characterized by the slip direction vector, $s^{(\alpha)}_i$,

and the vector normal to the slip plane, $m_i^{(\alpha)}$.

The slip increment, $\dot{\gamma}^{(\alpha)}$, is unrestricted with respect to sign, such that both positive and negative slip increments may occur. This results in the evolution of the slip; $\gamma^{(\alpha)} = \int_0^t \dot{\gamma}^{(\alpha)} \mathrm{d}t$. Dissipation of energy is assumed to be associated with the accumulation of statistically stored dislocations (SSDs), while recoverable energy is associated with the build up of geometrically necessary dislocations (GNDs) (Ashby, 1970). Thus, the accumulated slip; $\gamma_{acc}^{(\alpha)} = \int_0^t |\dot{\gamma}^{(\alpha)}| \mathrm{d}t$ is related to dissipation, while the net Burgers vector density, $\gamma_{,i}^{(\alpha)} s_i^{(\alpha)}$ is related to recoverable energy. A gradient enhanced effective slip is defined by the quadratic relation

$$\gamma_{eff}^{(\alpha)} = \sqrt{\left(\gamma^{(\alpha)}\right)^2 + l^2 \left(\gamma_{,i}^{(\alpha)} s_i^{(\alpha)}\right)^2} \tag{4}$$

where a single length parameter, l, governs the gradient dependence.

A power law hardening relation is adopted, such that; $\bar{\tau}_0^{(\alpha)}[\gamma] = \tau_y^{(\alpha)} + \hat{\tau}_0^{(\alpha)}[\gamma]$ is the conventional shear hardening curve defined in terms of the initial slip resistance, $\tau_y^{(\alpha)}$, and $\hat{\tau}_0^{(\alpha)}[\gamma] = \tau_y^{(\alpha)}\, k^{(\alpha)}\, \gamma^n$, is the slip dependent shear hardening curve defined by a strength coefficient, $k^{(\alpha)}$, and the hardening exponent, n. The total work expended in the material is

$$U[\varepsilon_{ij}^e, \gamma^{(:)}, \gamma_{,i}^{(:)} s_i^{(:)}] = \frac{1}{2}\, \sigma_{ij}\, \varepsilon_{ij}^e + \sum_{(\alpha)} U^{p^{(\alpha)}}[\gamma_{eff}^{(\alpha)}, \gamma_{acc}^{(\alpha)}] \tag{5}$$

in which the plastic contribution to the work expended, on the individual slip system, is defined by one of the two expressions:

Model A

$$\begin{aligned} U^{p^{(\alpha)}}[\gamma_{eff}^{(\alpha)}] &= \int_0^{\gamma_{eff}^{(\alpha)}} \bar{\tau}_0^{(\alpha)}[\gamma] \mathrm{d}\gamma \\ &= \tau_y^{(\alpha)} \left(\gamma_{eff}^{(\alpha)} + \frac{k^{(\alpha)}}{n+1} \left(\gamma_{eff}^{(\alpha)}\right)^{(n+1)}\right) \end{aligned} \tag{6}$$

Model B

$$
\begin{aligned}
U^{p^{(\alpha)}}[\gamma_{eff}^{(\alpha)}] &= \int_0^{|\gamma^{(\alpha)}|} \bar{\tau}_0^{(\alpha)}[\gamma]\mathrm{d}\gamma + \int_{|\gamma^{(\alpha)}|}^{\gamma_{eff}^{(\alpha)}} \hat{\tau}_0^{(\alpha)}[\gamma]\mathrm{d}\gamma \\
&= \tau_y^{(\alpha)} \left(|\gamma^{(\alpha)}| + \frac{k^{(\alpha)}}{n+1} \left(\gamma_{eff}^{(\alpha)}\right)^{(n+1)} \right) \qquad (7)
\end{aligned}
$$

Equations (6) and (7) are similar to their isotropic contourparts defined by Fleck et al. (2015), and their essential difference lies in the fact that the contribution from the net Burgers vector density does not affect the lowest order term in Eq. (7). The two models may be condensed in a unifying formalism by introducing the substitutional function $\tau_0^{(\alpha)}[*]$, which will represent $\bar{\tau}_0^{(\alpha)}[*]$ in the case of Model A and $\hat{\tau}_0^{(\alpha)}[*]$ in the case of Model B. An exception is the expressions for the micro-stress, derived assuming monotonic loading, which differ as shown in Eqs. (13) and (14). In the conventional limit ($l = 0$ and $\gamma_{acc}^{(\alpha)} = \gamma_{eff}^{(\alpha)}$), the plastic energy contribution is given by; $U^{p^{(\alpha)}}[\gamma_{acc}^{(\alpha)}] = \int_0^{\gamma_{acc}^{(\alpha)}} \bar{\tau}_0^{(\alpha)}[\gamma]\mathrm{d}\gamma$, which is recovered by both Eqs. (6) and (7). On the other hand, with $l > 0$, where gradients contribute to the material behavior, an energy surplus can be identified in both Eqs. (6) and (7) as

$$
\psi^{(\alpha)} = U^{p^{(\alpha)}}[\gamma_{eff}^{(\alpha)}] - U^{p^{(\alpha)}}[|\gamma^{(\alpha)}|] = \int_{|\gamma^{(\alpha)}|}^{\gamma_{eff}^{(\alpha)}} \tau_0^{(\alpha)}[\gamma]\mathrm{d}\gamma \qquad (8)
$$

when substituting the function $\tau_0^{(\alpha)}[*]$ in Eq. (8), for $\bar{\tau}_0^{(\alpha)}[*]$ and $\hat{\tau}_0^{(\alpha)}[*]$ to obtain the energy surplus for Model A and Model B, respectively. This energy surplus is here defined as a recoverable quantity through the definition of the net Burgers vector density evolution (with the evolution of slip gradients $\gamma_{,i}^{(\alpha)} = \int_0^t \dot{\gamma}_{,i}^{(\alpha)}\mathrm{d}t$).

The definition of the energy contributions allows the model specific stress quantities to be derived. Through the additive split of the micro-stress, the recoverable part is identified by; $q^{R(\alpha)} = \frac{\partial \psi^{(\alpha)}}{\partial \gamma^{(\alpha)}}$ and the dissipative micro-stress is; $q^{D(\alpha)} = \frac{\partial U^p[\gamma_{acc}]}{\partial \gamma^{(\alpha)}} = \bar{\tau}_0^{(\alpha)}[\gamma_{acc}]\,\mathrm{sgn}[\dot{\gamma}^{(\alpha)}]$. Thus, the total micro-stress is given

by

$$q^{(\alpha)} = \frac{\partial U}{\partial \gamma^{(\alpha)}} = \overbrace{\tau_0^{(\alpha)}[\gamma_{eff}^{(\alpha)}]\,\frac{\gamma^{(\alpha)}}{\gamma_{eff}^{(\alpha)}} - \tau_0^{(\alpha)}[|\gamma^{(\alpha)}|]\,\mathrm{sgn}[\gamma^{(\alpha)}]}^{q^{R(\alpha)}} + \overbrace{\bar{\tau}_0^{(\alpha)}[\gamma_{acc}^{(\alpha)}]\,\mathrm{sgn}[\dot{\gamma}^{(\alpha)}]}^{q^{D(\alpha)}}$$
$$\text{for} \quad \gamma^{(\alpha)} \neq 0 \quad \text{and} \quad \dot{\gamma}^{(\alpha)} \neq 0 \tag{9}$$

The derivatives $\frac{\partial|\gamma^{(\alpha)}|}{\partial\gamma^{(\alpha)}} = \mathrm{sgn}[\gamma^{(\alpha)}]$, for $\gamma^{(\alpha)} \neq 0$ and $\frac{\partial\gamma_{acc}^{(\alpha)}}{\partial\gamma^{(\alpha)}} = \mathrm{sgn}[\dot{\gamma}^{(\alpha)}]$, for $\dot{\gamma}^{(\alpha)} \neq 0$, where $\mathrm{sgn}[*]$ denotes the sign function, makes the recoverable micro-stress undefined in the case of $\gamma^{(\alpha)} \neq 0$ and the dissipative micro-stress undefined in the case of $\dot{\gamma}^{(\alpha)} \neq 0$. Before initial yield of a material point this is of no consequence since the microforce equilibrium equation (Eq. (2)) is not valid for such a material point. In practical terms during a general loading history these restrictions are of little consequence since the sign of the affected terms do not need to be updated unless a jump across zero is encountered for either variable. A detailed discussion of the micro-stress derivation can be found in Nellemann et al. (2017), which also includes an explanation as to how the the principle of dissipation (also known as the Clausius-Duhem inequality), $q^{D(\alpha)}\,\dot{\gamma}^{(\alpha)} \geq 0$, introduces a dependence on the sign of the slip increment $\dot{\gamma}^{(\alpha)}$.

In the present models the higher order stress is purely recoverable, hence, defined by

$$\xi^{(\alpha)} = \frac{\partial U}{\partial\left(\gamma_{,i}^{(\alpha)} s_i^{(\alpha)}\right)} = \tau_0^{(\alpha)}[\gamma_{eff}^{(\alpha)}]\frac{l^2\,\gamma_{,i}^{(\alpha)} s_i^{(\alpha)}}{\gamma_{eff}^{(\alpha)}} \tag{10}$$

2.2. Incremental framework assuming monotonic loading

The incremental framework is, here, restricted to monotonic loading to preserve the key characteristics relevant to the present investigation, while simplifying the implementation procedure. This restriction implies that; $|\gamma^{(\alpha)}| = \gamma_{acc}^{(\alpha)}$ and $\mathrm{sgn}[\dot{\gamma}^{(\alpha)}] = \mathrm{sgn}[\gamma^{(\alpha)}]$. The incremental contribution from the accumulated slip on the individual slip system is; $\dot{\gamma}_{acc}^{(\alpha)} = |\dot{\gamma}^{(\alpha)}|$, and the increment of the net Burgers vector density is; $\dot{\gamma}_{,i}^{(\alpha)} s_i^{(\alpha)}$. From Eq. (4), the incremental effective slip

can be derived as

$$\dot{\gamma}_{eff}^{(\alpha)} = \frac{\dot{\gamma}^{(\alpha)}\gamma^{(\alpha)} + l^2\,\gamma_{,i}^{(\alpha)}\,s_i^{(\alpha)}\,\dot{\gamma}_{,j}^{(\alpha)}\,s_j^{(\alpha)}}{\gamma_{eff}^{(\alpha)}} \tag{11}$$

In the isotropic plasticity theories by Fleck et al. (2015), two effective plastic strain quantities (generalized effective plastic strain in their terminology) are defined; one is a recoverable effective plastic strain on non-incremental form, and one is an unrecoverable (dissipative) effective plastic strain on incremental form. The effective slip defined in the present work can be viewed as a recoverable effective plastic strain in flow theory terminology, while this distinction is indefinable in the current context of deformation theory (monotonic loading). Furthermore, the expression in Eq. (11) is singular at the onset of plastic flow, which will be discussed further in relation to the finite element solution procedure in Section 3.2.

The incremental form of the elastic strain, $\dot{\varepsilon}_{ij}^{e}$, follows the non-incremental counterpart, thus, the elastic strain increment is given by; $\dot{\varepsilon}_{ij}^{e} = \dot{\varepsilon}_{ij} - \dot{\varepsilon}_{ij}^{p}$, with increments of the total strain given by; $\dot{\varepsilon}_{ij} = \frac{1}{2}\left(\dot{u}_{i,j} + \dot{u}_{j,i}\right)$, while increments of plastic strain is; $\dot{\varepsilon}_{ij}^{p} = \sum_{(\alpha)} \dot{\gamma}^{(\alpha)}\mu_{ij}^{(\alpha)}$. Through the elastic strain relation, the increment of Cauchy stress is

$$\dot{\sigma}_{ij} = L_{ijkl}^{e}\left(\dot{\varepsilon}_{kl} - \sum_{(\beta)} \dot{\gamma}^{(\beta)}\mu_{kl}^{(\beta)}\right) \tag{12}$$

with the incremental resolved shear stress given by; $\dot{\tau}^{(\alpha)} = \dot{\sigma}_{ij}\mu_{ij}^{(\alpha)}$. The assumption of monotonic loading simplifies the micro-stress expression given in Eq. (9), which results in two different expressions for the micro-stress

Model A (Based on Eq. (6))

$$q^{(\alpha)} = \bar{\tau}_0^{(\alpha)}[\gamma_{eff}^{(\alpha)}]\frac{\gamma^{(\alpha)}}{\gamma_{eff}^{(\alpha)}} \tag{13}$$

Model B (Based on Eq. (7))

$$q^{(\alpha)} = \hat{\tau}_0^{(\alpha)}[\gamma_{eff}^{(\alpha)}]\frac{\gamma^{(\alpha)}}{\gamma_{eff}^{(\alpha)}} + \tau_y\,\mathrm{sgn}[\gamma^{(\alpha)}] \quad \text{for} \quad \gamma^{(\alpha)} \neq 0. \tag{14}$$

The second term of Eq. (14) does not contribute to the incremental micro-stress, thus, either expression for the micro-stress results in the incremental micro-stress

$$\dot{q}^{(\alpha)} \quad = \quad h^{(\alpha)}[\gamma_{eff}^{(\alpha)}]\dot{\gamma}_{eff}^{(\alpha)}\frac{\gamma^{(\alpha)}}{\gamma_{eff}^{(\alpha)}} + \tau_0^{(\alpha)}[\gamma_{eff}^{(\alpha)}]\left(\frac{\dot{\gamma}^{(\alpha)}}{\gamma_{eff}^{(\alpha)}} - \dot{\gamma}_{eff}^{(\alpha)}\frac{\gamma^{(\alpha)}}{\gamma_{eff}^{(\alpha)^2}}\right) \tag{15}$$

Here, the hardening moduli are defined by $h^{(\alpha)}[\gamma_{eff}^{(\alpha)}] = \frac{\partial \tau_0^{(\alpha)}[\gamma_{eff}^{(\alpha)}]}{\partial \gamma_{eff}^{(\alpha)}}$, which only accounts for self-hardening. This choice of hardening law neglects latent hardening, which in the present work is chosen in order to clearly distinguish the effects that govern hardening (i.e. conventional strain hardening and the hardening contribution associated with gradients of slip). Thus, based on the objectives stated in the introduction any shear hardening relation (hardening law) that increases monotonically could be used for the two models presented.

The incremental higher order stress follows directly from Eq. (10), such that either model leads to the incremental higher order stress

$$\dot{\xi}^{(\alpha)} \quad = \quad l^2 s_i^{(\alpha)}\left(h^{(\alpha)}[\gamma_{eff}^{(\alpha)}]\dot{\gamma}_{eff}^{(\alpha)}\frac{\gamma_{,i}^{(\alpha)}}{\gamma_{eff}^{(\alpha)}} + \tau_0^{(\alpha)}[\gamma_{eff}^{(\alpha)}]\left(\frac{\dot{\gamma}_{,i}^{(\alpha)}}{\gamma_{eff}^{(\alpha)}} - \dot{\gamma}_{eff}^{(\alpha)}\frac{\gamma_{,i}^{(\alpha)}}{\gamma_{eff}^{(\alpha)^2}}\right)\right) \tag{16}$$

The principle of virtual work on incremental form is

$$\int_V \left(\dot{\sigma}_{ij}\delta\dot{\varepsilon}_{ij} + \sum_{(\alpha)}\left(\dot{q}^{(\alpha)} - \dot{\tau}^{(\alpha)}\right)\delta\dot{\gamma}^{(\alpha)} + \sum_{(\alpha)}\dot{\xi}^{(\alpha)}s_i^{(\alpha)}\delta\dot{\gamma}_{,i}^{(\alpha)}\right)\mathrm{d}V = \int_S\left(\dot{T}_i\delta\dot{u}_i + \sum_{(\alpha)}\dot{r}^{(\alpha)}\delta\dot{\gamma}^{(\alpha)}\right)\mathrm{d}S \tag{17}$$

with the volume of the solid V, the surface S, and δ denoting variational quantities. The incremental surface tractions, work conjugate to increments of displacements, and the incremental higher order surface tractions, work conjugate to the increments of slips, are $\dot{T}_i = \dot{\sigma}_{ij}\,n_j$ and $\dot{r}^{(\alpha)} = \dot{\xi}^{(\alpha)}\,s_j^{(\alpha)}\,n_j$, respectively, with n_j denoting the unit outward normal to S.

The initial yield condition of the rate-independent strain gradient crystal plasticity framework follows the conventional crystal plasticity yield criterion,

on individual slip systems, such that $\tau^{(\alpha)} = \tau_y^{(\alpha)}$. A key assumption related to the behavior of the material is that only the Cauchy stress, σ_{ij}, is assumed to change during elastic deformation (discussed in detail by Hutchinson (2012) in relation to isotropic plasticity).

3. Numerical method

The two models have been implemented in a 2D plane strain finite element code, with increments of displacement and increments of slip as free variables. The variational quantities and field quantities are discretized using polynomial interpolation functions, where the combination of quadratic elements for the displacement field and bi-linear elements for the plastic slip field is adopted.

3.1. Finite element discretization

Eight node quadratic isoparametric elements are used to interpolate increments of nodal displacements, $\dot{d}^M$, such that 16 shape functions, N_i^M, are employed in 2D. Thus, increments of displacements and increments of strains can be written as

$$\dot{u}_i = \sum_{M=1}^{16} N_i^M \, \dot{d}^M \quad \text{and} \quad \dot{\varepsilon}_{ij} = \sum_{M=1}^{16} E_{ij}^M \, \dot{d}^M \tag{18}$$

with $E_{ij}^M = \frac{1}{2}(N_{i,j}^M + N_{j,i}^M)$. The superscript upper-case Latin letters represent elements in one and two dimensional arrays in the present section, with the exception of T which indicate the transpose of a matrix. Four node linear isoparametric elements are used to interpolate increments of nodal slips, $\dot{g}^{(\alpha)N}$, with 4 shape functions, $M^{(\alpha)N}$ (equal for all slip systems). Thus, increments of slip and their spatial gradients read

$$\dot{\gamma}^{(\alpha)} = \sum_{N=1}^{4} M^{(\alpha)N} \, \dot{g}^{(\alpha)N} \quad \text{and} \quad \dot{\gamma}_{,i}^{(\alpha)} = \sum_{N=1}^{4} M_{,i}^{(\alpha)N} \, \dot{g}^{(\alpha)N} \tag{19}$$

The system of equations, which follows from discretizing Eq. (17), takes the form

$$\begin{bmatrix} \left[K_e\right] & \left[K_{ep}^{(\alpha)}\right] \\ \left[K_{ep}^{(\alpha)}\right]^T & \left[K_p^{(\alpha,\beta)}\right] \end{bmatrix} \begin{Bmatrix} \left\{\dot{d}\right\} \\ \left\{\dot{g}^{(\alpha)}\right\} \end{Bmatrix} = \begin{Bmatrix} \left\{F_1\right\} \\ \left\{F_2^{(\alpha)}\right\} \end{Bmatrix} \tag{20}$$

with the three matrices $\left[K_e\right]$, $\left[K_{ep}^{(\alpha)}\right]$ and $\left[K_p^{(\alpha,\beta)}\right]$ identified as:

(i) The conventional elastic stiffness matrix

$$\left[K_e\right]^{MN} = \int_V L_{ijkl}^e E_{kl}^M E_{ij}^N \mathrm{d}V \tag{21}$$

(ii) Elastic-plastic matrices which couple nodal increments of displacements and nodal increments of slip

$$\left[K_{ep}^{(\alpha)}\right]^{NM} = -\int_V L_{ijkl}^e \mu_{kl}^{(\alpha)} M^{(\alpha)M} E_{ij}^N \mathrm{d}V \tag{22}$$

(iii) Slip system matrices which couple nodal increments of slip, either on an individual slip system ($\alpha = \beta$) or across two different slip systems ($\alpha \neq \beta$)

$$\begin{aligned}
\left[K_p^{(\alpha,\beta)}\right]^{MN} &= \int_V \mu_{ij}^{(\alpha)} L_{ijkl}^e \mu_{kl}^{(\beta)} M^{(\beta)M} M^{(\alpha)N} \mathrm{d}V \\
&+ \delta_{\alpha\,\beta} \int_V \left(\left(h^{(\alpha)}[\gamma_{eff}^{(\alpha)}] - \frac{\tau_0^{(\alpha)}[\gamma_{eff}^{(\alpha)}]}{\gamma_{eff}^{(\alpha)}} \right) \frac{\gamma^{(\alpha)^2}}{\gamma_{eff}^{(\alpha)^2}} + \frac{\tau_0^{(\alpha)}[\gamma_{eff}^{(\alpha)}]}{\gamma_{eff}^{(\alpha)}} \right) M^{(\alpha)M} M^{(\alpha)N} \, \mathrm{d}V \\
&+ \delta_{\alpha\,\beta} \int_V \left(h^{(\alpha)}[\gamma_{eff}^{(\alpha)}] - \frac{\tau_0^{(\alpha)}[\gamma_{eff}^{(\alpha)}]}{\gamma_{eff}^{(\alpha)}} \right) \frac{\gamma^{(\alpha)}}{\gamma_{eff}^{(\alpha)^2}} l^2 \, s_i^{(\alpha)} \gamma_{,i}^{(\alpha)} s_j^{(\alpha)} \left(M_{,j}^{(\alpha)M} M^{(\alpha)N} + M^{(\alpha)M} M_{,j}^{(\alpha)N} \right) \mathrm{d}V \\
&+ \delta_{\alpha\,\beta} \int_V \left(\left(h^{(\alpha)}[\gamma_{eff}^{(\alpha)}] - \frac{\tau_0^{(\alpha)}[\gamma_{eff}^{(\alpha)}]}{\gamma_{eff}^{(\alpha)}} \right) \frac{\left(l^2 \, s_i^{(\alpha)} \gamma_{,i}^{(\alpha)} \right)^2}{\gamma_{eff}^{(\alpha)^2}} + l^2 \frac{\tau_0^{(\alpha)}[\gamma_{eff}^{(\alpha)}]}{\gamma_{eff}^{(\alpha)}} \right) s_j^{(\alpha)} M_{,j}^{(\alpha)M} s_k^{(\alpha)} M_{,k}^{(\alpha)N} \, \mathrm{d}V
\end{aligned} \tag{23}$$

where $\delta_{\alpha\,\beta}$ is the Kronecker delta. The right-hand side of Eq. (20) contains two contributions; $\left\{F_1\right\}$ related to conventional tractions, and $\left\{F_2^{(\alpha)}\right\}$ related to higher-order tractions. These are defined by

$$\left\{F_1\right\}^M = \int_S \dot{T}_i N_i^M \mathrm{d}S \tag{24}$$

$$\left\{F_2^{(\alpha)}\right\}^N = \int_S \dot{r}^{(\alpha)} M^{(\alpha)N} \mathrm{d}S \tag{25}$$

In the special case of single slip ($\alpha = \beta = 1$), the combined element matrix in Eq. (20) is comprised of; (i) the elastic stiffness matrix (16 x 16 in size), (ii) the elastic-plastic coupling matrix (4 x 16), and (iii) the slip system matrix

(4 x 4). By extending the system to multiple active slip systems, additional coupling matrices appear, compared to the single slip case, and the combined element matrix in Eq. (20) is then comprised of additional elastic-plastic coupling matrices and slip system coupling matrices. Essentially, four additional nodal slip variables appear per element for each additional slip system. Despite, being derived in terms of a forward (explicit) Euler solution scheme the presented tangent stiffness matrix is identical to the so-called consistent tangent stiffness matrix commonly derived from equations that define divergence from equilibrium (i.e. the residual).

3.2. Numerical implementation

An in-house 2D plane strain finite element code, that includes both models, has been developed. The external package SuiteSparse (Davis et al., 2014) is used through the framework PETSc (Balay et al., 2015) in order to solve the sparse linear system of equations. Throughout, the conventional Gauss quadrature rule is used for numerical integration, with 3×3 Gauss point for both the 8 node elements (full integration) that discretizes the displacement field and the 4 node elements (over integration) for the plastic slip field.

In the proposed rate-independent models, initial yielding is evaluated on Gauss point basis, such that the element stiffness may consist of both elastic and elastic-plastic contributions. In non-active plastic Gauss points, $\left[K_{ep}^{(\alpha)}\right]$ and $\left[K_{p}^{(\alpha,\beta)}\right]$ is set equal to zero when evaluating the combined element stiffness matrix. However, if a slip system is determined non-active in all Gauss points, belonging to a specific element, the stiffness matrix contributions from $\left[K_{p}^{(\alpha,\beta)}\right]$, for $\alpha = \beta$, are set equal to the identity matrix multiplied by a sufficiently large value (in the present work $10^7 \times G$, with G being the shear modulus). This is essentially a penalty approach which ensures zero slip increments on a specific slip system of that element. As a result some Gauss points of the element which are by definition in the plastic regime may not attain a non-zero value of the slip increment, such that the elastic-plastic boundary reflects a steep transition when moving from an elastic region into a plastic region. Physically this bound-

ary condition may be interpreted as a constraint on the plastic flow which blocks the motion of dislocations at the moving elastic plastic interface (a micro-hard boundary). An alternative to penalizing the slip in this manner, which results in a micro-free boundary, has been discussed by Martnez-Paeda and Niordson (2016) and Niordson and Hutchinson (2003)

The discrete finite element mesh used to obtain all results consists of a single column of 1000 square elements through the height H (see Section 4 for a complete description of the boundary value problem analyzed). The incremental solution schemes for the two models differ to the extent that each is described separately.

Model A (the case of $\tau_0^{(\alpha)} = \bar{\tau}_0^{(\alpha)}$) is solved using 10,000 imposed displacement steps of equal magnitude, and convergence of the solution using a forward Euler scheme is found. In Nellemann et al. (2017) it is reported that a numerical initialization procedure is needed to overcome the singular behavior of several terms in Eq. (23) at initial yield. The approach chosen to overcome this numerical issues is to start calculations with a small value of initial slip throughout the entire body. The initial slip value used in the present work is $\gamma^{(\alpha)} = \gamma_{eff}^{(\alpha)} = 2 \times 10^{-3}\, \gamma_y^{(\alpha)}$, with the reference strain measure given as $\gamma_y^{(\alpha)} = \tau_y^{(\alpha)}/G$. The effect of this initialization procedure is demonstrated by Nellemann et al. (2017) for the case of single slip in an infinite crystalline slab subjected to pure shear deformation (equivalent to the boundary value problem investigated in the present work). Nellemann et al. (2017) found that the deviation between results for the value $\gamma^{(\alpha)} = \gamma_{eff}^{(\alpha)} = 2 \times 10^{-3}\, \gamma_y^{(\alpha)}$ and the lowest possible value at which a solution was obtainable, is below 1% for a representative range of length parameter values.

Model B (the case of $\tau_0^{(\alpha)} = \hat{\tau}_0^{(\alpha)}$) is solved using 1000 imposed displacement steps, initially of equal magnitude. However, an iterative yield point approach scheme is used to determine the value of the displacement which results in yielding. Due to the specifics of the boundary value problem analysed, the scheme iterates to fulfill the condition $0.0 < |\tau_y^{(:)}| - \hat{\tau}_0^{(:)} \leq 1 \times 10^{-8}$ for all Gauss points in the domain. When the condition violates the upper limit the imposed dis-

placement increment is scaled by the value 0.9^m , with m initialized to zero (at the beginning of the step) and increasing by one each subsequent violation of the condition during that specific step. When the condition is fulfilled the remaining part of the displacement increment is added to the next displacement increment and the incremental solution is recovered. Furthermore, since $\frac{\hat{\tau}_0^{(\alpha)}[\gamma_{eff}^{(\alpha)}]}{\gamma_{eff}^{(\alpha)}} = h^{(\alpha)}[\gamma_{eff}^{(\alpha)}] = \tau_y^{(\alpha)}\, k^{(\alpha)}$, for the case of hardening exponent $n = 1$ (linear hardening), the slip system matrices that couple nodal increments of slip (Eq. (23)) reduce to

$$\begin{aligned}\left[K_p^{(\alpha,\beta)}\right]^{MN} &= \int_V \mu_{ij}^{(\alpha)} L_{ijkl}^{e} \mu_{kl}^{(\beta)} M^{(\beta)M} M^{(\alpha)N} \mathrm{d}V \\ &+ \delta_{\alpha\,\beta} \int_V \tau_y^{(\alpha)}\, k^{(\alpha)} \left(M^{(\alpha)M} M^{(\alpha)N} + l^2\, s_j^{(\alpha)} M_{,j}^{(\alpha)M} s_k^{(\alpha)} M_{,k}^{(\alpha)N} \right) \mathrm{d}V \end{aligned} \tag{26}$$

eliminating the need for a numerical initialization procedure. As a consequence, no gradient effects contribute to the element stiffness matrix in the limit of $\tau_y^{(\alpha)}\, k^{(\alpha)} = h^{(\alpha)} \to 0$. Furthermore, an alternative way of deriving Model B in this limit could be through several additive contributions to the plastic work

$$\begin{aligned} U^{p^{(\alpha)}}[|\gamma^{(\alpha)}|, \gamma_{,i}^{(\alpha)} s_i^{(\alpha)}] &= \int_0^{|\gamma^{(\alpha)}|} \bar{\tau}_0^{(\alpha)}[\gamma]\mathrm{d}\gamma + \int_0^{l\,\gamma_{,i}^{(\alpha)} s_i^{(\alpha)}} \hat{\tau}_0^{(\alpha)}[\gamma'_{,i} s_i]\mathrm{d}[\gamma'_{,i} s_i] \\ &= \tau_y^{(\alpha)} \left(|\gamma^{(\alpha)}| + \frac{k^{(\alpha)}}{2} \left(\gamma_{eff}^{(\alpha)} \right)^2 \right) \end{aligned} \tag{27}$$

which resembles the plastic work suggested by Fleck et al. (2015) in the context of eliminating strengthening behavior in strain gradient theories.

4. Pure shear of a crystalline strip

A crystalline strip of material with height H and width W, confined between rigid platens and subject to monotonic pure shear loading, is considered as benchmark problem (see Fig. 1). The edges parallel to the x_1-axis are bonded to rigid platens, and in order to model an infinite strip the conventional boundary conditions are

$$u_2 = 0 \quad \text{on} \quad x_2 = \pm H/2 \quad \text{and} \quad \text{on} \quad x_1 = \pm W/2 \tag{28}$$

$$u_1 = \pm \Delta/2 \quad \text{on} \quad x_2 = \pm H/2 \tag{29}$$

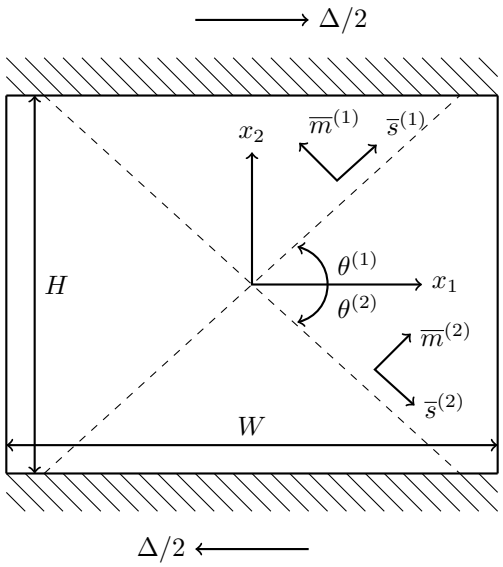

Figure 1: Illustration of a crystalline strip of height H and width W. The strip is subjected to pure shear loading through the applied displacements $\Delta/2$ acting parallel to the x_1-axis (indicated by arrows). The material is elastic-plastic, with two slip systems defined by the slip direction vectors, $\overline{s}^{(\alpha)}$, and the vectors normal to the slip plane, $\overline{m}^{(\alpha)}$, (with the slip planes indicated by dashed lines). The slip systems are inclined by the angle $\theta^{(1)} = -\theta^{(2)} = \theta$ relative to the x_1-axis, resulting in the relation $\overline{s}^{(1)} = (\cos(\theta), \sin(\theta)) = \overline{m}^{(2)}$, $\overline{s}^{(2)} = (\cos(\theta), -\sin(\theta))$ and $\overline{m}^{(1)} = (-\cos(\theta), \sin(\theta))$. Micro-hard boundary conditions, blocking the motion of dislocations, are applied onto the top and the bottom of the strip for $l > 0$.

with the shear, Δ, prescribed incrementally in the finite element analysis. Additionally, horizontal periodicity of displacement and slips is prescribed

$$u_1[-W/2, x_2] = u_1[W/2, x_2] \tag{30}$$

$$\gamma^{(\alpha)}[-W/2, x_2] = \gamma^{(\alpha)}[W/2, x_2] \quad \text{for all } \alpha \tag{31}$$

while the edges parallel to the x_1-axis are assumed micro-hard for $l > 0$

$$\gamma^{(\alpha)} = 0 \quad \text{on} \quad x_2 = \pm H/2 \tag{32}$$

300 The material is elastic-plastic, with the ratio between the initial slip resistance and the shear modulus given by $\tau_y^{(\alpha)}/G = 0.0104$ and Poisson's ratio $\nu = 0.3$. Linear strain hardening characterizes the material (n = 1), with the normalized

conventional strain hardening parameter $h/G = 0.2$ (unless otherwise stated).

The model based on the plastic work defined in Eq. (7) (Model B) can be treated analytically for the case of monotonic pure shear loading, since it predicts a proportional straining history (related results are presented and discussed in Section 5). The pure shear loading of an infinite strip is essentially a one dimensional boundary value problem for the slip variables and the horizontal displacement, given in terms of the uniform distribution of the resolved shear stress imposed on the strip (see Bittencourt et al., 2003, for details). The boundary value problem with field quantities independent of x_1 and the only non-zero Cauchy stress components being $\sigma_{12} = \sigma_{21}$ define the solutions of interest. The case of symmetric double slip, with $\theta^{(1)} = -\theta^{(2)} = \theta$ (as illustrated in Fig. 1), and the special case of a single slip system with the slip system orientation angle $\theta = 90^\circ$ fall within the solutions of interest. The conventional equilibrium condition (in Eq. (1)) requires σ_{12} to be spatially uniform. This results in yielding throughout the entire strip at the exact same load increment, when yield is defined as in the case of conventional crystal plasticity (noted in Section 2.2). However, as discussed by Fleck et al. (2015) (for the case of isotropic strain gradient plasticity) the onset of plastic flow may not arise when $\tau^{(\alpha)} = \tau_y^{(\alpha)}$. Fleck et al. (2015) use the term elastic loading gap to characterize this behavior, which is termed strengthening in the present work. The conditions reported by Fleck et al. (2015): $\frac{\partial U^{p^{(\alpha)}}[\gamma_{eff}^{(\alpha)}]}{\partial \gamma^{(\alpha)}} = \tau_y^{(\alpha)}$ and $\frac{\partial U^{p^{(\alpha)}}[\gamma_{eff}^{(\alpha)}]}{\partial\left(\gamma_{,i}^{(\alpha)} s_i^{(\alpha)}\right)} = 0$ at $\gamma^{(\alpha)} = 0$ and $\gamma_{,i}^{(\alpha)} s_i^{(\alpha)} = 0$ must be fulfilled, under monotonic and positive loading, to ensure that strengthening does not arises in either model. This condition is fulfilled for Model B , however, Model A results in $\frac{\partial U^{p^{(\alpha)}}[\gamma_{eff}^{(\alpha)}]}{\partial \gamma^{(\alpha)}} = \tau_y^{(\alpha)} \frac{\gamma^{(\alpha)}}{\gamma_{eff}^{(\alpha)}}$ and $\frac{\partial U^{p^{(\alpha)}}[\gamma_{eff}^{(\alpha)}]}{\partial\left(\gamma_{,i}^{(\alpha)} s_i^{(\alpha)}\right)} = \tau_y^{(\alpha)} \frac{l^2 \gamma_{,i}^{(\alpha)} s_i^{(\alpha)}}{\gamma_{eff}^{(\alpha)}}$ at $\gamma^{(\alpha)} = 0$ and $\gamma_{,i}^{(\alpha)} s_i^{(\alpha)} = 0$, hence strengthening must be expected for this model. However, as noted in Section 2.2 the Cauchy stress alone defines yielding of the material, which leads to the definition of the apparent rise in yield limit being a property related to plasticity in the case of rate-independence.

In the remainder of this work, all parameters related to plasticity are pre-

sented without a superscript Greek letter slip system identifier, since these will be assumed equal for the cases of symmetric double slip and only one exists for the case of single slip.

4.1. An exact closed form solution to pure shear loading conditions

The analytical solutions will be restricted to characterize plastic behavior, neglecting material behavior prior to yielding. Monotonic positive slip is assumed, such that $\text{sgn}[\gamma] = 1$ and $s_2 = \sin(\theta)$, resulting in the reduced expression for the effective slip

$$\gamma_{eff} = \sqrt{\gamma^2 + l^2 \, (\gamma_{,2} s_2)^2} \tag{33}$$

For the boundary value problem at hand, the micro-stress, defined by Eq. (14), and the higher order stress, in Eq. (10), reduce to

$$q^{(\alpha)} = \hat{\tau}_0[\gamma_{eff}] \frac{\gamma}{\gamma_{eff}} + \tau_y \tag{34}$$

$$\xi^{(\alpha)} = \hat{\tau}_0[\gamma_{eff}] \frac{l^2 \, \gamma_{,2} s_2}{\gamma_{eff}} \tag{35}$$

with the directional derivative of the higher order stress given by

$$\xi_{,2} \, s_2 = l^2 s_2^2 \left(\left(h[\gamma_{eff}] - \frac{\hat{\tau}_0[\gamma_{eff}]}{\gamma_{eff}} \right) \frac{\left(\gamma \, (\gamma_{,2})^2 + l^2 \, s_2 \, \gamma_{,2} \, \gamma_{,22} \right)}{(\gamma_{eff})^2} + \frac{\gamma_{,22} \, \hat{\tau}_0[\gamma_{eff}]}{\gamma_{eff}} \right) \tag{36}$$

Inserting Eq. (34) and Eq. (36) into the microforce equilibrium equation (in Eq. (2)), and assuming linear hardening, results in

$$-\lambda^2 \gamma_{,22} + \gamma = F \tag{37}$$

where

$$\lambda = l \, s_2 \quad \text{and} \quad F = \frac{(\tau - \tau_y)}{h} \tag{38}$$

This expression for the governing ordinary differential equation of the specific boundary value problem is very similar to the one obtained by Bittencourt

et al. (2003) for their proposed rate-independent strain gradient crystal plasticity formulation. The analytical solution of the conventional crystal plasticity formulation (the limit $l = 0$, where microscopic boundary conditions cannot be imposed), can be obtained by imposing the boundary conditions; $\gamma_{,2} = 0$ at $x_2 = \pm H/2$ on Eq. (37). This results in a uniform slip across the material slab given by; $\gamma = F$. However, the solution to Eq. (37) for $l > 0$ is subject to the boundary conditions in Eq. (32), which results in the more complex slip distribution given by

$$\gamma = F\left(1 - \frac{\cosh(x_2/\lambda)}{\cosh(H/(2\lambda))}\right) \tag{39}$$

The expressions for the slip distribution and the distribution of the spatial gradient of slip will be compared to the finite element solutions in Section 5.

The distributions of the first and second spatial derivative of the slip in the x_2-direction follow by differentiating Eq. (39), and result in

$$\gamma_{,2} = -F\frac{\sinh(x_2/\lambda)}{\lambda\cosh(H/(2\lambda))} \tag{40}$$

and

$$\gamma_{,22} = -F\frac{\cosh(x_2/\lambda)}{\lambda^2\cosh(H/(2\lambda))} \tag{41}$$

The average slip through the height of the strip is given by

$$\gamma_{(avg.)} = \frac{1}{H}\int_{-H/2}^{H/2}\gamma\,\mathrm{d}x_2 = F\left(1 - \tanh(H/(2\lambda))\frac{2\lambda}{H}\right) \tag{42}$$

which can be used to identify the normalized average effective hardening modulus

$$\frac{h_{eff}}{h} = \frac{F}{\gamma_{(avg.)}} = \frac{H}{H - 2\lambda\tanh(H/(2\lambda))} \tag{43}$$

The definition of F indicates that the limit $h \to 0$ is singular, such that the above expressions for the slip distribution, the slip gradient distribution and the average slip are unbounded. However, the average effective hardening modulus is independent of the conventional shear hardening parameter, and expressed purely in terms of λ (i.e. the slip system orientation angle and the length parameter) and the strip height H. The expression for the effective hardening modulus is compared to finite element predictions in Section 5.

5. Results and discussion

In the present work, strengthening is defined as an apparent delay in plastic flow, while hardening is defined by the combined effect of conventional strain hardening and the additional hardening owing to strain gradients. The results presented consist of finite element predictions which for Model B, are compared to the analytical solutions derived in Section 4.1. The case of single slip (with $\theta = 90°$) will be used to present hardening and strengthening characteristics of the two formulations, while hardening predictions for both single slip and symmetric double slip ($\theta = 15°$ and $30°$, respectively) conclude the results section.

Results of single slip ($\theta = 90°$) are presented in Figs. 2 - 9, where predictions of strengthening and hardening behavior of the two models are compared. The influence of the length scale parameter on the shear stress-strain curves is shown in Fig. 2. It is seen that both formulations reduce to the conventional limit when $l \to 0$, while an increase in hardening is predicted for increasing values of l/H. It is worth noticing that Model A predicts strengthening and a slightly non-linear post yielding material response despite employing a linear hardening model, and both effects are found to intensify with increasing l/H. In contrast, Model B predicts linear hardening and no strengthening for the same set of parameters. The slip profile amplitude through the straining history is shown in Fig. 3 for both models. The predictions of Model A are non-linear in the plastic regime, indicating a non-proportional straining history (see Hutchinson, 2012, for details on proportional straining in the case of isotropic strain gradient plasticity). Contrary to this, Model B predicts a piecewise linear evolution of the slip profile amplitude, which indicates that proportional straining occurs at a single material point of the strip in the plastic regime. The proportional straining history predicted by Model B is further substantiated in Figure 4 where the normalized slip profile through the top half of the crystalline strip, at various stages of deformation, is shown for the case of $l/H = 0.8$. The stages of deformation are presented as percentages of the plastic strain imposed at

the final stage of deformation $\varepsilon_p^f = \frac{\Delta^f}{H} - \frac{\tau_y}{G}$, with $\Delta^f/H = 0.086$. The non-proportional straining history predicted by Model A is confirmed in Figure 4. The plastic strain essentially evolves from the initialization value and is highly affected by the effect of strengthening. However, the slip profile of Model A converges towards that of Model B as the plastic deformation is increased (this has been confirmed by enforcing a deformation of $\Delta^f/H = 0.86$). The results presented in Figs. 2 - 4 substantiate the key objectives for "proper model development" proposed by Hutchinson (2012) (restated in the introduction of the present work). In the case of Model A objective one and two are met, however objective three is not, while all three objectives are met for Model B.

Predictions of slip profile distributions, for various values of l/H, at the overall shear strain (Δ^f/H) are presented in Fig. 5. The limit $l/H = 0$ is approached by the curves for $l/H = 0.01$, which is reflected by a uniform distribution of the slip throughout most of the strip height and sharp boundary layers at the edges of the domain. The predicted slip is seen to decrease in overall magnitude for increasing l/H, and the strengthening predicted by Model A is reflected through a noticeable smaller magnitude of the slip distribution when compared to the predictions of Model B and the analytical solution presented in Eq. (39).

The associated slip gradient distributions are shown in Figs. 6(a) and 6(b). The result obtained for $l/H = 0.01$ shows a highly localized slip gradient distribution at the boundaries, for both models, and the results predicted by Model B and the analytical solution presented in Eq. (40) coincide. The results of both models for $l/H = 0.4$ and 0.8 are representative of the gradual change in slip gradient distribution for the interval $l/H = 0.01 - 0.8$. The value $l/H = 0.8$ marks a transition which is reflected by the results of $l/H = 1.6$, displaying an overall decreases in magnitude for both models. In the case of Model A, almost no change in distribution is seen as l/H is increased from 0.4 to 0.8, while a further increase results in a close to linear distribution near the the boundaries in combination with a distinct change in distribution away from the boundaries. As the length parameter is increased from 0.4 to 0.8 Model B approaches

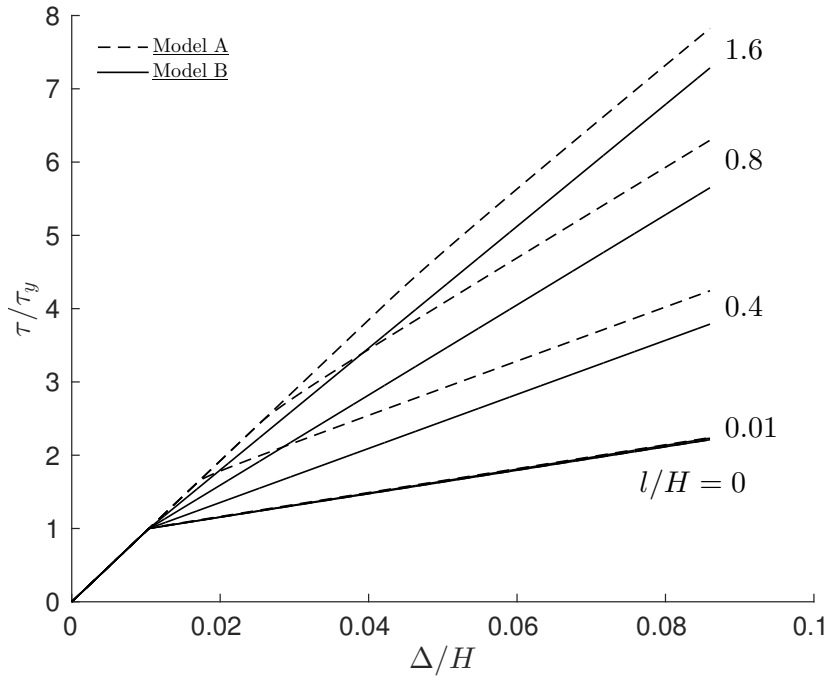

Figure 2: Shear stress-strain response to the imposed overall shear strain Δ/H, for single slip ($\theta = 90°$), and for various values of the normalized length parameter l/H. The normalized conventional strain hardening parameter is $h/G = 0.2$. The curves are obtained using Model A and Model B.

an almost linear distribution, which decreases in over all magnitude as l/H is increased further.

The influence of the conventional strain hardening parameter on the resolved shear stress predictions of the two models is shown in Fig. 7, for the case of $l/H = 0.4$. The predictions of Model B display no strengthening behavior and a linear hardening response, and with an apparently ideally plastic material behavior predicted for $h/G = 5 \times 10^{-5}$. Similarly, the predictions of Model A show response curves with similar slopes, however, both strengthening and a slight curvature of the post yielding material response is observed. Furthermore, the strengthening predictions of Model A are seen to be independent of conventional strain hardening which is consistent with several other strain gradi-

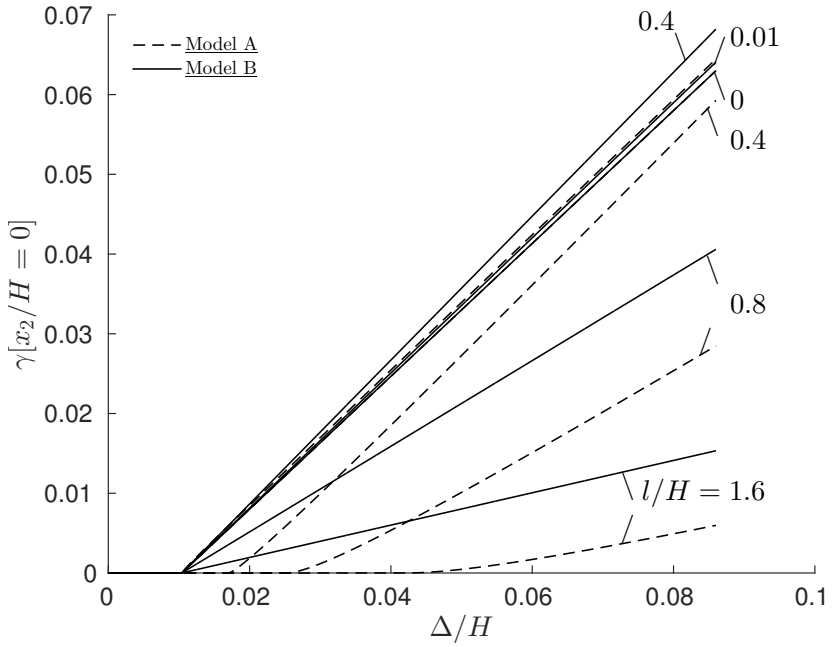

Figure 3: Slip profile amplitude to the imposed overall shear strain Δ/H, for single slip ($\theta = 90°$), and for various values of the normalized length parameter l/H. The normalized conventional strain hardening parameter is $h/G = 0.2$. The curves are obtained using Model A and Model B.

ent theories exhibiting strengthening (e.g. Fredriksson and Gudmundson, 2005; Lele and Anand, 2008; Niordson and Legarth, 2010). Figure 8 shows the associated slip profiles for the two formulations and the analytical solution presented in Eq. (39). The result obtained using Model A displays boundary layers that increase in magnitude for decreasing values of $h/G \leq 5 \times 10^{-3}$, and with very sharp boundary layers for $h/G = 5 \times 10^{-5}$. The predictions of Model B show an increase in slip throughout the height of the strip for decreasing values of h/G. Furthermore, perfect agreement is found between Model B and the analytical solution, which has been accurately obtained by the adopted yield point approach scheme (see Section 3.2). The predicted slip gradient distributions are presented in Fig. 9. The data plotted is restricted to the interval between $l\,\gamma_{,2}\,s_2 = -0.5$ and $l\,\gamma_{,2}\,s_2 = 0.5$ on the normalized slip gradient axis, such that

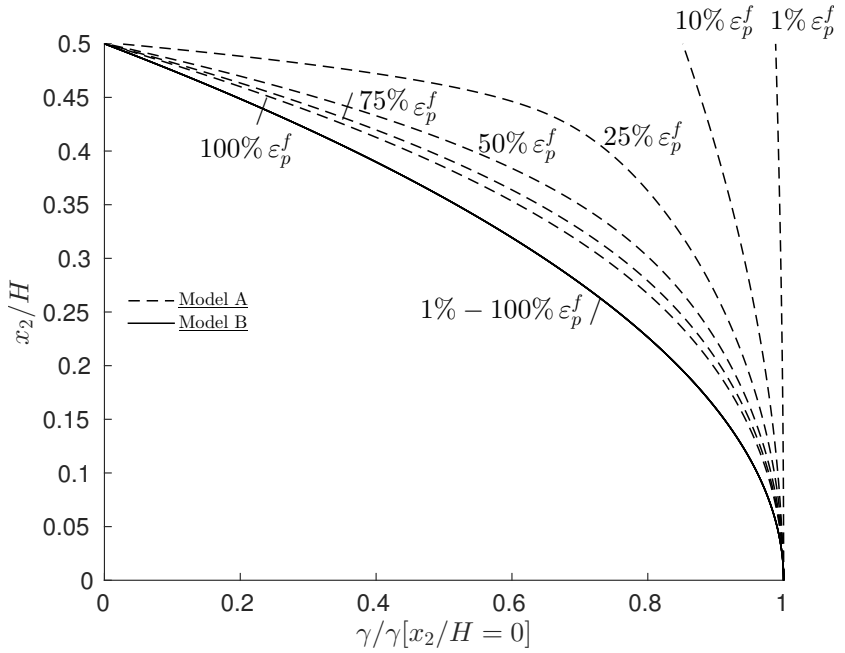

Figure 4: The normalized slip profile, $\gamma/\gamma[x_2/H = 0]$, through half the height of the strip at various stages of deformation. The stages of plastic strain are presented as percentages of the plastic strain, given by $\varepsilon_p^f = \frac{\Delta^f}{H} - \frac{\tau_y}{G}$, imposed at the final stage of deformation, $\frac{\Delta^f}{H}$. The curves are obtained using Model A and Model B for single slip ($\theta = 90^\circ$), and the normalized length parameter is $l/H = 0.8$. The normalized conventional strain hardening parameter is $h/G = 0.2$.

a visual comparison is possible. In the case of Model A, the cutoff interval excludes the peak values of the normalized slip gradient for $h/G = 5 \times 10^{-3}$ and $h/G = 5 \times 10^{-5}$ which are determined to 0.5158 and 3.932, respectively. As seen, sharp peaks and high concentrations of slip gradient profile are predicted for these values of conventional strain hardening. The results predicted by Model B show almost linear distributions, which increase slightly in overall magnitude for decreasing values of h/G. The results of the analytical solution is again in perfect agreement with the results of Model B (especially notice the zoom included). A comparison of the slip gradient profiles associated with various values of l/H and h/G (Fig. 6 and Fig. 9) indicates that a highly lo-

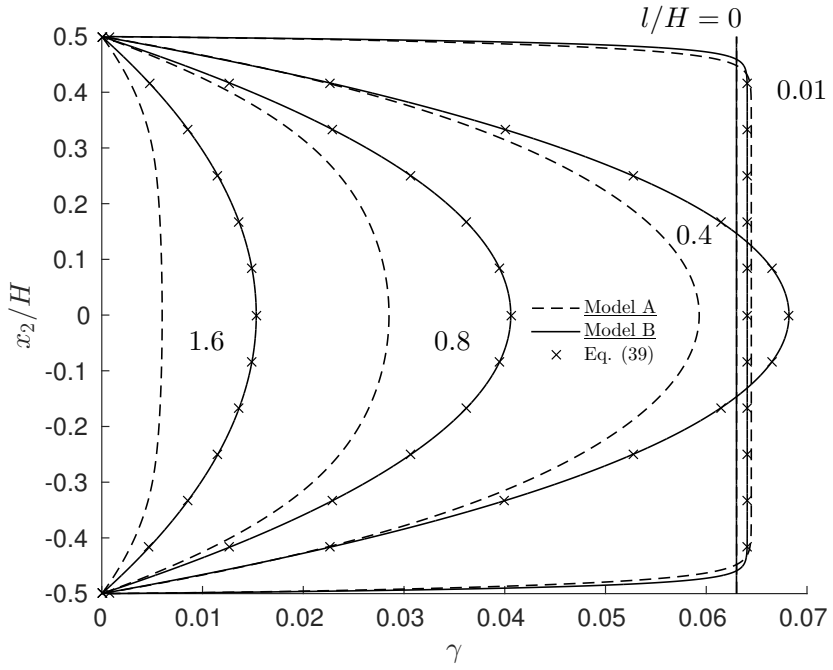

Figure 5: Slip profile, γ, at imposed overall shear strain; $\Delta^f/H = 0.086$, for single slip ($\theta = 90°$), and for various values of the normalized length parameter l/H. The normalized conventional strain hardening parameter is $h/G = 0.2$. The curves are obtained using Model A and Model B, while the markers are obtained using Eq. (39).

calized slip gradient distribution is predicted by Model A at the boundaries for low values of either the length parameter or the conventional strain hardening parameter. While Model B only shows the same trend for low values of l/H.

The analytical solution for the hardening, derived in Section 4.1, is based on the definition of the plastic work in Eq. (7). This solution is valid for the case of symmetric double slip and the special case of single slip with the slip system orientation angle $\theta = 90°$. Furthermore, as noted in relation to Eq. (43), the hardening enhancement over conventional strain hardening is independent of h, and depends only on the length parameter, the slip direction vector component s_2, and the height of the strip. In order to quantify the hardening behavior, Figure 10 presents the normalized average effective hardening modulus, $h_{eff}/h = (\tau - \tau_y)/(\gamma_{(avg.)}h)$, as a function of a slip system orien-

tation dependent length parameter defined by; $2\,ls_2/H$, to compare results for various cases. The slip direction vector component s_2 is constant for a given choice of slip system orientation and l is the slip system orientation dependent length parameter. The results of Model A and Model B are obtained using the normalized conventional strain hardening parameter ($h/G = 0.2$), but the numerical results have been found to be independent of non-zero values of h/G. The markers on the curve represent discrete data point values, for three values of slip system orientation angle ($\theta = 15°$, $30°$ and $90°$, respectively), and the solid line is given by Eq. (43). In the case of proportional straining history the expression $h_{eff}/h = (\tau[\Delta^f_{100\%}] - \tau_y)/(\gamma_{(avg.)}[\Delta^f_{100\%}]h)$, with $\Delta^f_{100\%}$ referring to the percentage of overall imposed shear strain, is sufficient to evaluate the effective hardening moduli. However, due to the non-proportional straining history predicted by Model A, the effective hardening moduli are calculated using data points at 90 % and 100 % of the imposed overall shear strain (in this case being $\Delta^f/H = 0.172$, or twice the overall shear strain otherwise used in the present work). Thus, the effective hardening moduli for Model A are evaluated using $h_{eff}/h = (\tau[\Delta^f_{100\%}] - \tau[\Delta^f_{90\%}])/((\gamma_{(avg.)}[\Delta^f_{100\%}] - \gamma_{(avg.)}[\Delta^f_{90\%}])h)$. It is seen from Fig. 10 that the predictions of both Model A and Model B coincide with the analytical solution, confirming that Model A converges towards proportional straining as the effects due to strengthening become negligible (also indicated by the findings related to Fig. 3 and 4) and that the effective hardening relation is independent of the conventional strain hardening parameter. Further details on the strengthening behavior of Model A are presented in the work of Nellemann et al. (2017) which, also, includes a figure showing the magnitude of the predicted strengthening as a function of the normalized length parameter.

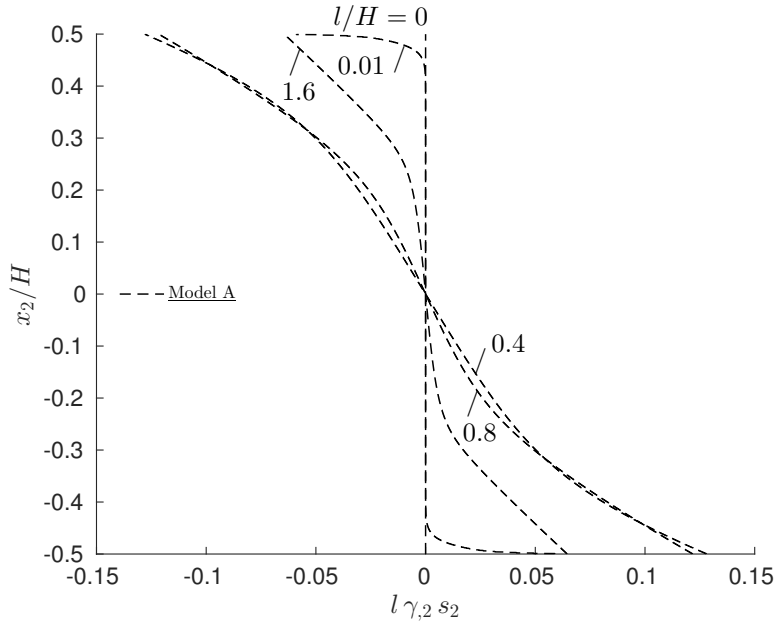

(a) Curves obtained using Model A.

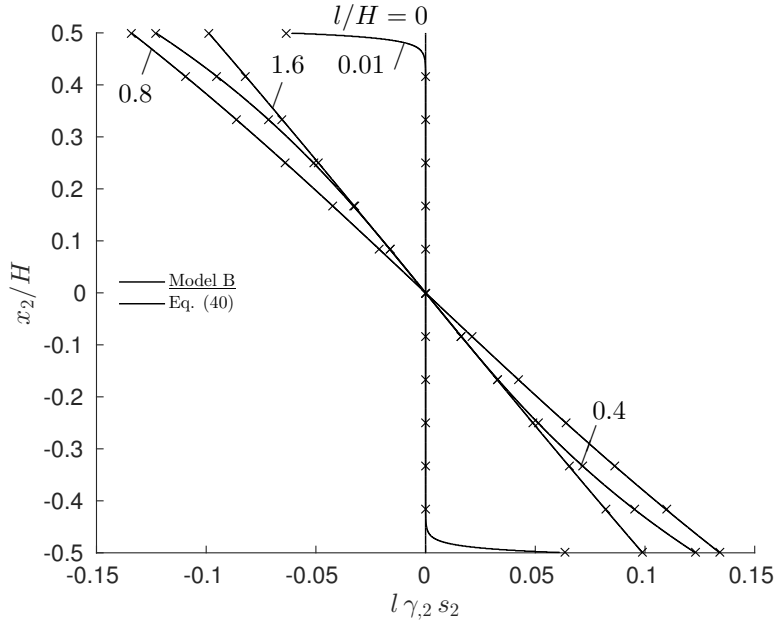

(b) Curves obtained using Model B and markers obtained using Eq. (40).

Figure 6: Normalized slip gradient profile, $l\,\gamma_{,2}\,s_2$, at imposed overall shear strain $\Delta^f/H = 0.086$, for single slip ($\theta = 90°$), and for various values of the normalized length parameter l/H. The normalized conventional strain hardening parameter is $h/G = 0.2$.

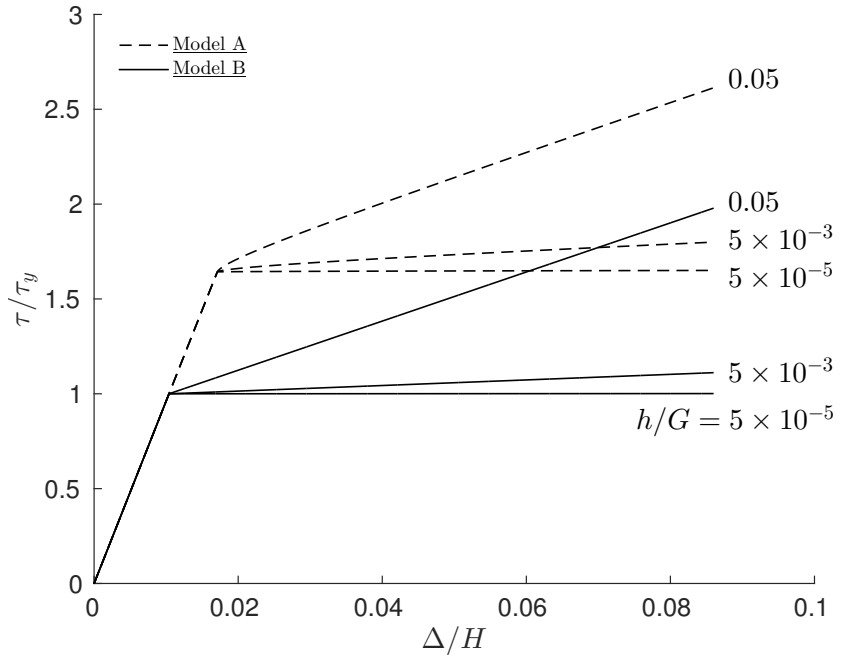

Figure 7: Shear stress-strain response to the imposed overall shear strain Δ^f/H, for single slip ($\theta = 90°$), and for various values of the normalized conventional strain hardening parameter h/G. The normalized length parameter is $l/H = 0.4$. The curves are obtained using Model A and Model B.

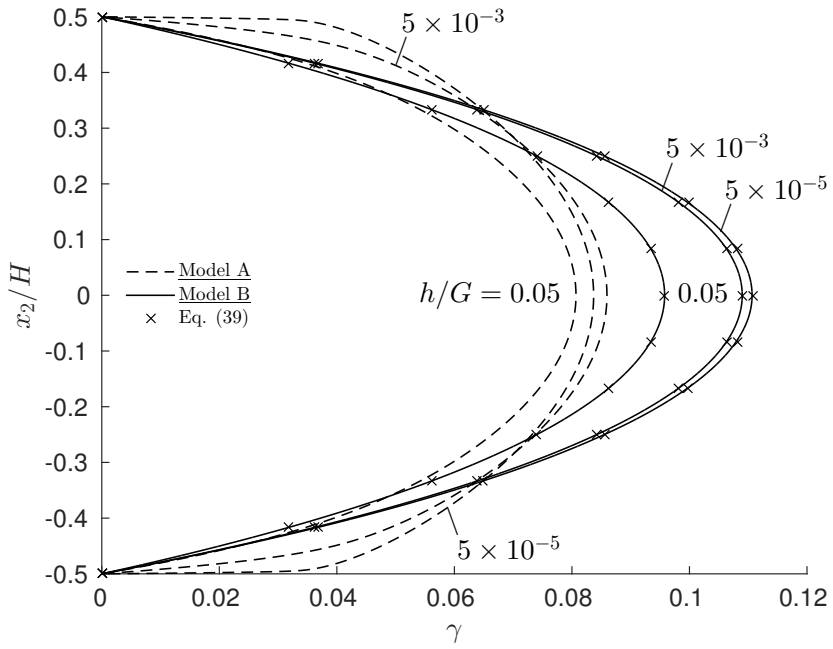

Figure 8: Slip profile, γ, at imposed overall shear strain $\Delta^f/H = 0.086$, for single slip ($\theta = 90°$), and for various values of the normalized conventional strain hardening parameter h/G. The normalized length parameter is $l/H = 0.4$. The curves are obtained using Model A and Model B, while the markers are obtained using Eq. (39).

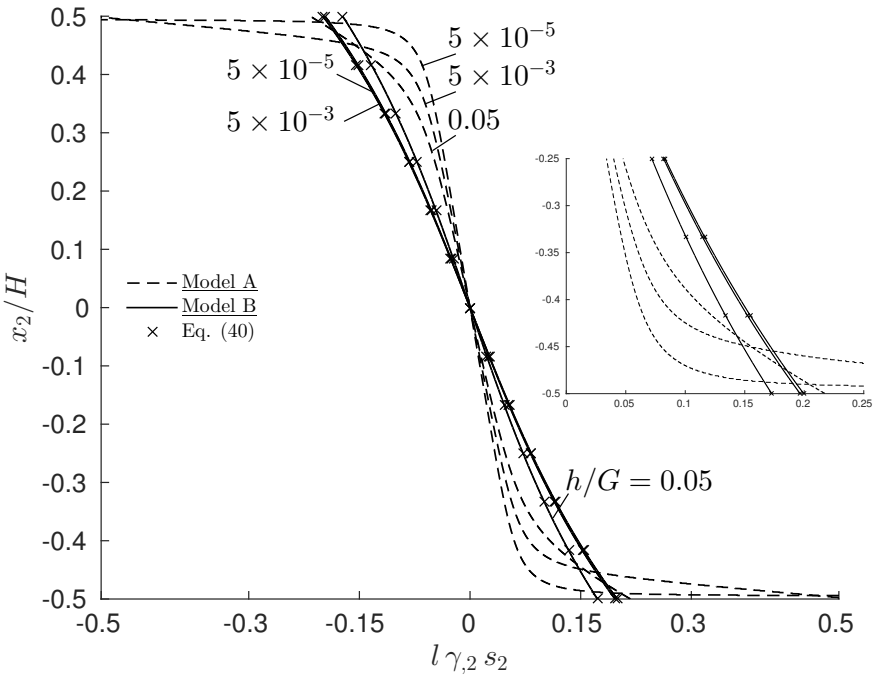

Figure 9: Normalized slip gradient profile, $l\,\gamma_{,2}\,s_2$, at imposed overall shear strain $\Delta^f/H = 0.086$, for single slip ($\theta = 90°$), and for various values of the normalized conventional strain hardening parameter h/G. The normalized length parameter is $l/H = 0.4$. The curves are obtained using Model A and Model B, while the markers are obtained using Eq. (40). A zoom of the results near the lower boundary is included.

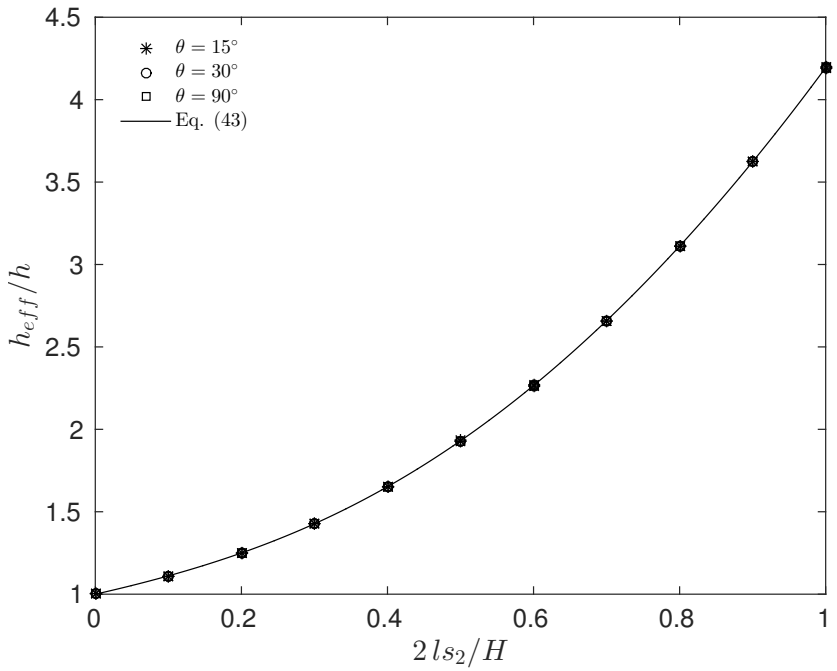

Figure 10: Effect of normalized length parameter $2ls_2/H$ on the normalized average effective hardening moduli $h_{eff}/h = (\tau - \tau_y)/(\gamma_{(avg.)}h)$. The markers represent solutions obtained by Model A and Model B, for three different values of slip system orientation angle ($\theta = 15°, 30°$ and $90°$) with the value of the normalized conventional strain hardening parameter $h/G = 0.2$. The solid line is plotted using the analytical expression in Eq. (43).

6. Concluding remarks

Two closely related rate-independent strain gradient crystal plasticity models have been presented in a unifying framework. Model A is investigated in the work of Nellemann et al. (2017), while the present work presents Model B and a comparison of the two models. The specific difference between the two models lies in whether or not the constant term of the conventional strain hardening curve is associated with gradients of slip in the definition of the plastic work. Essential to this difference is the issue of strengthening, as predicted by Fleck et al. (2015) for the case of isotropic plasticity.

Three objectives proposed by Hutchinson (2012) for "proper model development" are adopted in the present work. The first objective is met since both the models predict the response of conventional crystal plasticity theory in the limit of vanishing gradients. The second objective is also fulfilled for both models, as the unified framework is defined by elastic parameters (Poisson's ratio and the shear modulus), the plastic material response is defined in terms of a relation between resolved shear stress and slip (corresponding to the uni-axial tensile curve in isotropic plasticity), and a material length parameter that scales the gradient dependence. The third objective requires that deformation theory and flow theory coincides for a proportional straining history, which is fulfilled in the case of Model B, but not for Model A. Model A predicts a non-proportional straining history for the pure shear boundary value problem due to strengthening, which is found to be independent of the conventional strain hardening. An apparent consequence of this strengthening behavior is that Model A predicts a straining history which is approximately proportional when the overall shear strain is sufficiently large and the effect of the initial strengthening is negligible. Through deformation theory considerations an exact solution to the plastic behavior in an infinite slab subjected to pure shear is derived, based on the framework for Model B. The solution is shown to coincide with the prediction of Model B. Furthermore, an analytical expression for the effective hardening modulus is obtained, which reveals that the effective hardening modulus is in-

dependent of conventional strain hardening. The expression is even found to coincide with the predictions of Model A at deformation levels where the effects of strengthening are negligible.

The microscopic response predicted by the two models generally show differences in distributions of slip and net Burgers vector density, both in the case of varying values of the length parameter and the level of the conventional strain hardening parameter. In the case of Model A, increasingly sharp boundary layers are predicted for both the distribution of slip and the net Burgers vector density at low conventional strain hardening (Figs. 8 and 9). In contrast, much smaller changes in the distribution of the slip and the net Burgers vector density are predicted for varying conventional strain hardening using Model B (Figs. 8 and 9). When varying the length parameter, both models predict sharp boundary layers in the net Burgers vector density distribution for a small length parameter and vice-versa for intermediate length parameter values. A further increase in length parameter reveals that the distribution increases in overall magnitude until a transitional value is reached, at which further increase in length parameter results in an overall decreasing distribution (Fig. 6).

The incremental formulation is derived based on the assumption of monotonic loading. This simplifies the numerical model implementation and in combination with the use of linear conventional strain hardening, the strengthening and hardening characteristics of the two models are accentuated, both in terms of the results presented and the analytical treatment of Model B. Based on Model B a simplified expression for the slip system matrices that couple increments of nodal slip is obtained for linear conventional strain hardening (Eq. (26)), which is accompanied by a simplified expression for the plastic work (Eq. (27)). These expressions reveal that the predictions of Model B are those of a recoverable energy with a quadratic dependence on gradients of slip since the slip and slip gradients contribute independently to the plastic work. Contrary, to Model A where the slip and slip gradient contribution is coupled through the effective slip measure. The simplification of Model B for linear conventional strain hardening (Eq. (26)) further reveals that gradient contributions to the element stiffness

matrix are scaled by the conventional shear hardening modulus, such that the limit $h^{(\alpha)} = \tau_y^{(\alpha)}\, k^{(\alpha)} \to 0$ reduces the formulation to the perfectly plastic limit of conventional rate-independent crystal plasticity.

As noted in Section 3.2 the general expression for the slip system matrices that couple increments of nodal slip is singular at the onset of yield, which in the case of Model A is overcome by using a small initial value of the slip and in the case of Model B vanishes in the limit of linear conventional strain hardening. While the expression in Eq. (26) for Model B does not include cases of $n \neq 1$, it may be used in the first plastic load increment with the substitution $\tau_y^{(\alpha)}\, k^{(\alpha)} = h^{(\alpha)}[\gamma_{eff}^{(\alpha)} = 0]$ in the case of general loading.

The effect of strengthening that arises from strain gradients is significant at small material length scales (e.g. Liu et al., 2015). This effect is predicted by Model A, while no such effect is predicted by Model B for the choice of material parameters presented. This finding supports the fact that strengthening does not arise in strain gradient theories when a quadratic dependence on gradients of plastic strain is utilized (see Fleck et al., 2015). The presented models are phenomenologically based, however, assessed in light of these experimental findings Model A seems a better choice from a physical point of view. While this assessment is based entirely on the pure shear boundary value problem analyzed, further investigations of Model B predictions may reveal strengthening and other material micro structure characteristics when utilizing material parameters that preclude a quadratic dependence on gradients of strain.

7. Acknowledgments

This work is financially supported by The Danish Council for Independent Research through the research career program Sapere Aude. Grant 11-105098, "*Higher Order Theories in Solid Mechanics*". Furthermore, Professor John W. Hutchinson is gratefully acknowledged for his suggestions and comments on model development.

Ashby, M.F., 1970. The deformation of plastically non-homogeneous materials. Philosophical Magazine 21, 399–424. doi:10.1080/14786437008238426.

Balay, S., Abhyankar, S., Adams, M.F., Brown, J., Brune, P., Buschelman, K., Dalcin, L., Eijkhout, V., Gropp, W.D., Kaushik, D., Knepley, M.G., McInnes, L.C., Rupp, K., Smith, B.F., Zampini, S., Zhang, H., 2015. PETSc Users Manual. Technical Report ANL-95/11 - Revision 3.6. Argonne National Laboratory. URL: http://www.mcs.anl.gov/petsc.

Bittencourt, E., Needleman, A., Gurtin, M., der Giessen, E.V., 2003. A comparison of nonlocal continuum and discrete dislocation plasticity predictions. Journal of the Mechanics and Physics of Solids 51, 281 – 310. doi:http://dx.doi.org/10.1016/S0022-5096(02)00081-9.

Davis, T., Duff, I., Amestoy, P., Gilbert, J., Larimore, S., Natarajan, E.P., Chen, Y., W, H., Rajamanickam, S., 2014. SuiteSparse: a suite of sparse matrix packages. http://faculty.cse.tamu.edu/davis/suitesparse.html.

Fleck, N.A., Hutchinson, J.W., Willis, J.R., 2015. Guidelines for constructing strain gradient plasticity theories. Journal of Applied Mechanics 82. doi:10.1115/1.4030323.

Fredriksson, P., Gudmundson, P., 2005. Size-dependent yield strength of thin films. International Journal of Plasticity 21, 1834 – 1854. doi:http://dx.doi.org/10.1016/j.ijplas.2004.09.005.

Greer, J.R., Hosson, J.T.D., 2011. Plasticity in small-sized metallic systems: Intrinsic versus extrinsic size effect. Progress in Materials Science 56, 654 – 724. doi:http://dx.doi.org/10.1016/j.pmatsci.2011.01.005. festschrift Vaclav Vitek.

Guo, S., He, Y., Lei, J., Li, Z., Liu, D., 2017. Individual strain gradient effect on torsional strength of electropolished microscale copper wires. Scripta Materialia 130, 124 – 127. doi:http://dx.doi.org/10.1016/j.scriptamat.2016.11.029.

Gurtin, M.E., 2000. On the plasticity of single crystals: free energy, microforces, plastic-strain gradients. Journal of the Mechanics and Physics of Solids 48, 989 – 1036. doi:http://dx.doi.org/10.1016/S0022-5096(99)00059-9.

Hutchinson, J., 2012. Generalizing J_2 flow theory: Fundamental issues in strain gradient plasticity. Acta Mechanica Sinica 28, 1078–1086. doi:10.1007/s10409-012-0089-4.

Lele, S.P., Anand, L., 2008. A small-deformation strain-gradient theory for isotropic viscoplastic materials. Philosophical Magazine 88, 3655–3689. URL: http://dx.doi.org/10.1080/14786430802087031, doi:10.1080/14786430802087031.

Liu, D., He, Y., Shen, L., Lei, J., Guo, S., Peng, K., 2015. Accounting for the recoverable plasticity and size effect in the cyclic torsion of thin metallic wires using strain gradient plasticity. Materials Science and Engineering: A 647, 84 – 90. doi:http://dx.doi.org/10.1016/j.msea.2015.08.063.

Ma, Q., Clarke, D.R., 1995. Size dependent hardness of silver single crystals. Journal of Materials Research 10, 853–863. doi:10.1557/JMR.1995.0853.

Martnez-Paeda, E., Niordson, C., 2016. On fracture in finite strain gradient plasticity. International Journal of Plasticity 80, 154 – 167. doi:http://dx.doi.org/10.1016/j.ijplas.2015.09.009.

Mu, Y., Hutchinson, J., Meng, W., 2014. Micro-pillar measurements of plasticity in confined cu thin films. Extreme Mechanics Letters 1, 62 – 69. doi:http://dx.doi.org/10.1016/j.eml.2014.12.001.

Nellemann, C., Niordson, C., Nielsen, K., 2017. An incremental flow theory for crystal plasticity incorporating strain gradient effects. International Journal of Solids and Structures 110 - 111, 239 – 250. doi:http://doi.org/10.1016/j.ijsolstr.2017.01.025.

Niordson, C.F., Hutchinson, J.W., 2003. Non-uniform plastic deformation of micron scale objects. International Journal for Numerical Methods in Engineering 56, 961–975.

Niordson, C.F., Legarth, B.N., 2010. Strain gradient effects on cyclic plasticity. Journal of the Mechanics and Physics of Solids 58, 542 – 557. doi:10.1016/j.jmps.2010.01.007.